Asymptotic Stabilization of a Five-link, Four-Actuator, Planar Bipedal Runner: Additional Figures

C. Chevallereau

IRCCyN, Ecole Centrale de Nantes
UMR CNRS 6597, BP 92101
1 rue de la Noë, 44321 Nantes
cedex 03, France
E-mail: Christine.Chevallereau@irccyn.ec-nantes.fr

E.R. Westervelt

Department of Mechanical Engineering
The Ohio State University
Columbus, Ohio 43210, USA
E-mail: westervelt.4@osu.edu

J.W. Grizzle

Control Systems Laboratory
EECS Department
University of Michigan
Ann Arbor, Michigan 48109-2122, USA
E-mail: grizzle@umich.edu
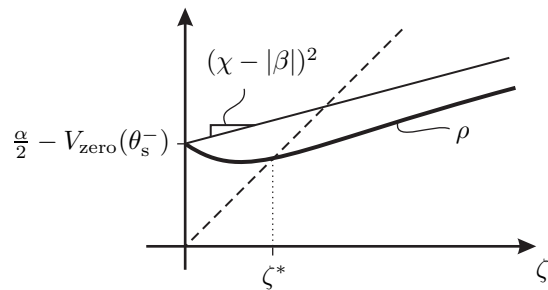
(a) stable
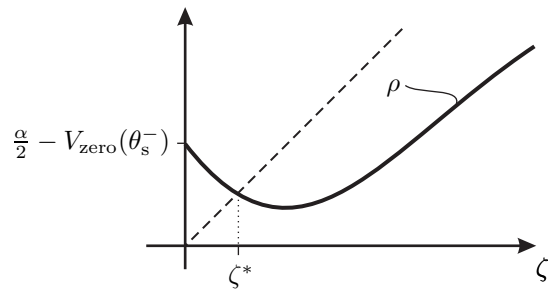
(b) unstable

Fig. 1. Sketches of example Poincaré maps for running.
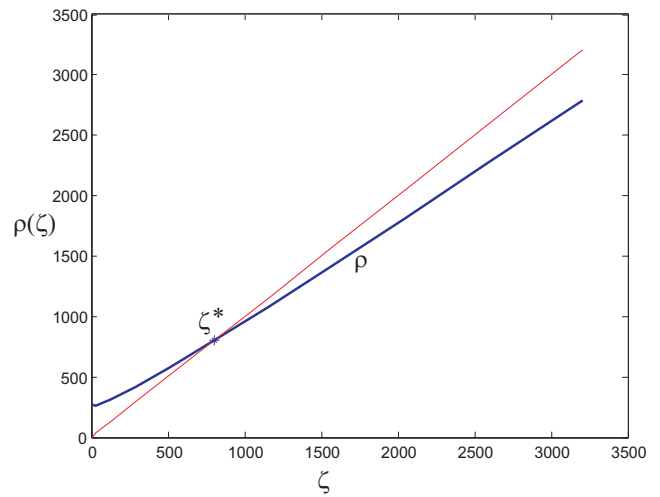
Fig. 2. The restricted Poincaré map associated with the closed-loop system. The fixed point occurs where ρ intersects the identity map, also shown.
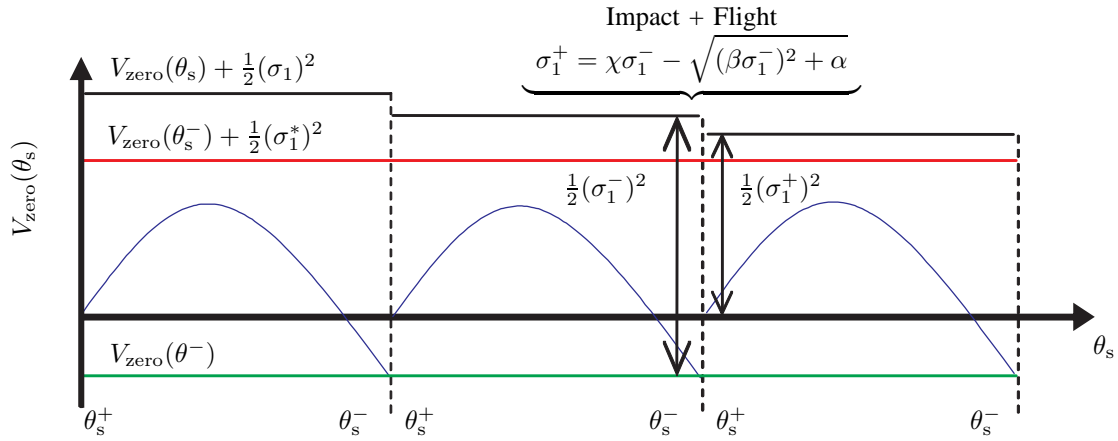
Fig. 3. The stance phase zero dynamics is Lagrangian, and thus throughout the stance phase, the corresponding total energy $V_{\text{zero}}(\theta_{\text{s}}) + \frac{1}{2}\sigma_1^2$ is constant. Over the impact plus flight phase, the change in total energy depends on the angular momentum through $\delta(\sigma_1^-)$ and the potential energy through $V_{\text{zero}}(\theta_{\text{s}}^-)$. The total energy corresponding to the periodic orbit is $V_{\text{zero}}(\theta_{\text{s}}^-) + \frac{1}{2}(\sigma_1^*)^2$.
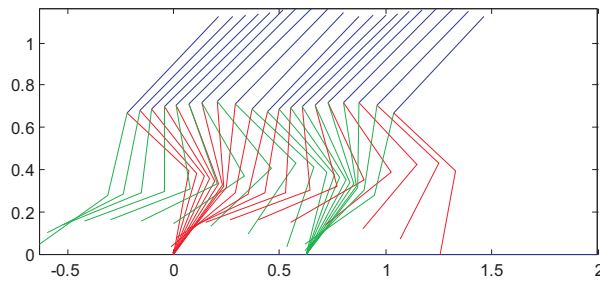
Fig. 4. Stick diagram for the running trajectory used to define the control law.
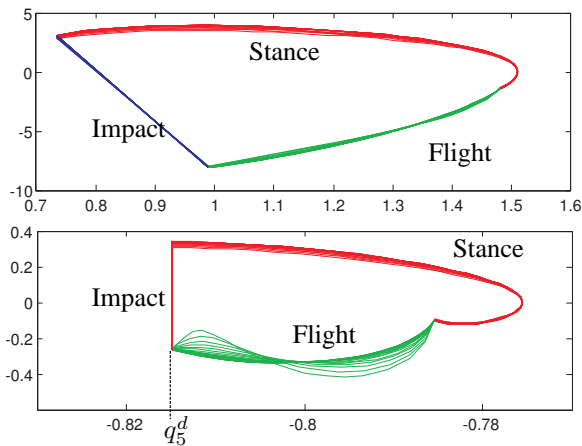
Fig. 5. The top graph depicts leg-1 (stance leg) knee angle (x-axis) versus its velocity (y-axis) in the stance and flight phases. The bottom graph depicts torso angle (x-axis) versus its velocity (y-axis) in the stance and flight phases. Notice that the flight-phase controller has regulated the torso angle to its desired value of q_5^d at impact. Both plots indicate that a limit cycle is achieved. In fact, the obtained limit cycle corresponds to the original periodic orbit, $\mathcal{O}$.
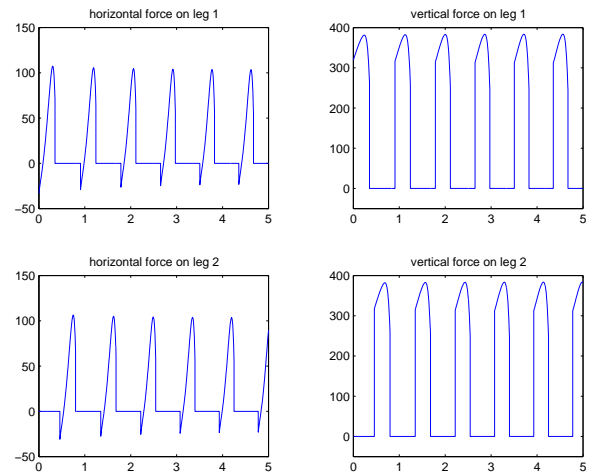
Fig. 6. Time (sec) versus ground reaction forces (N).
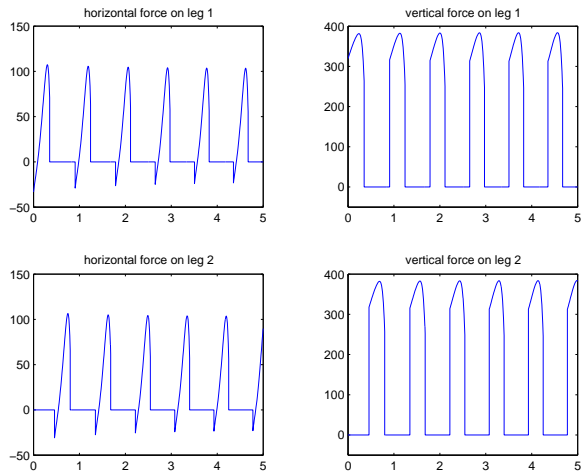
Fig. 7. Time (sec) versus joint torques (Nm).
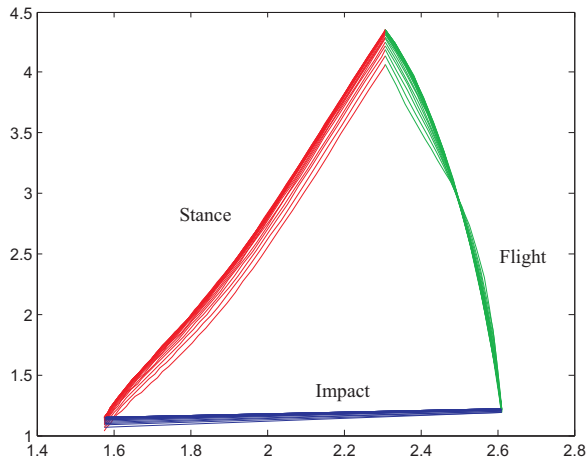
Fig. 8. Leg-1 (stance leg) hip angle (x-axis) versus its velocity in the stance and flight phases. The configuration of the robot is constant for each transition between phases. During the impact, the change of position corresponds to the commutation of the leg number.
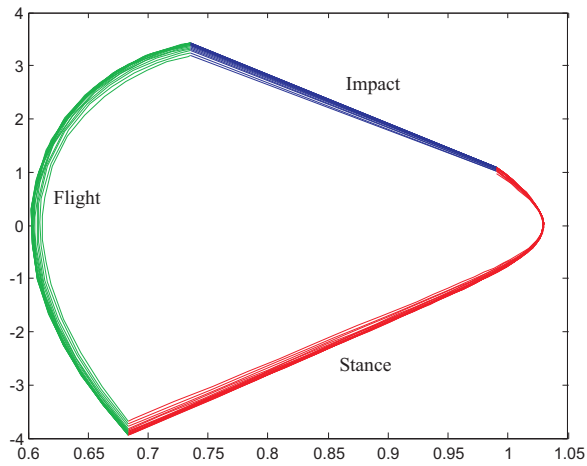
Fig. 9. Leg-1 (stance leg) knee angle (x-axis) versus its velocity in the stance and flight phases. The configuration of the robot is constant for each transition between phases. During the impact, the change of position corresponds to the commutation of the leg number.
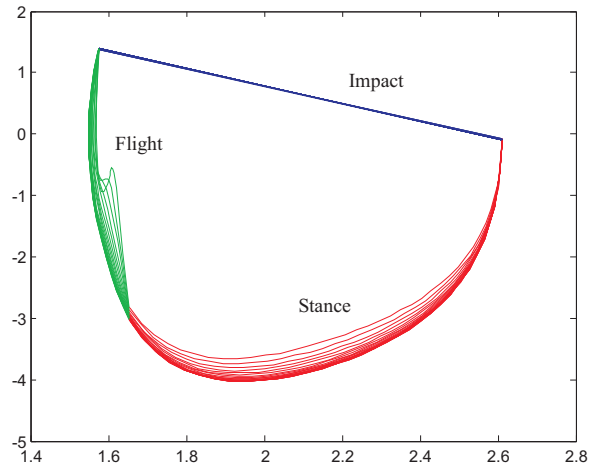
Fig. 10. Leg-2 (swing leg) hip angle (x-axis) versus its velocity in the stance and flight phases. The configuration of the robot is constant for each transition between phases. During the impact, the change of position corresponds to the commutation of the leg number.
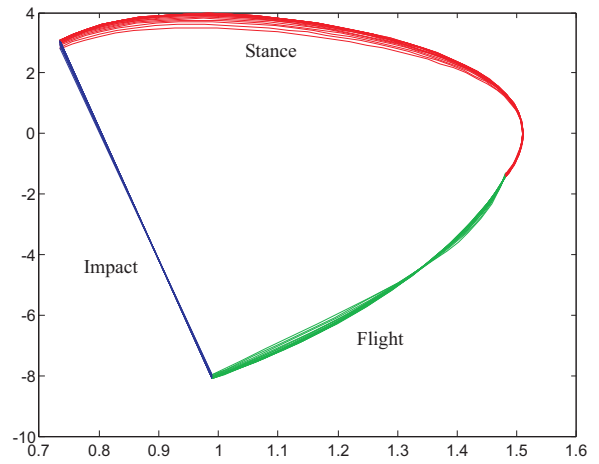
Fig. 11. Leg-2 (swing leg) knee angle (x-axis) versus its velocity in the stance and flight phases. The configuration of the robot is constant for each transition between phases. During the impact, the change of position corresponds to the commutation of the leg number.
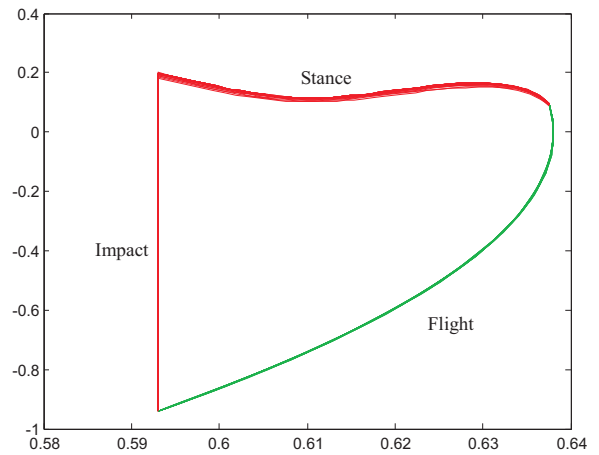
Fig. 12. Center of mass vertical displacement (m) versus center of mass horizontal displacement (m).